

Detection of single electronic spins by scanning tunnelling microscopy

C. DURKAN

Recent experimental advances now mean that it is possible to detect and probe single electronic spins with nanometre spatial resolution. This has implications for materials characterization at the single-atom level as well as for solid-state quantum computation. This paper focuses on the experimental issues regarding this technique, and on a simple model to explain the origin of the effect.

1. Introduction

In the 100 years since Stern and Gerlach experimentally confirmed Dirac's prediction of its existence, electron spin has become a fundamental property of matter of immense practical value, as has nuclear spin. The properties of electrons within atoms, molecules and solids are described using four *quantum numbers* [1]. These numbers contain information about the type of orbitals, (s, p, d, f, g or hybrids) the electrons reside in, as well as the magnetic moment due to the electron. The magnetic moment of electrons within materials has two components, as shown in figure 1: (1) an orbital contribution due to the fact that, except for the case of s-orbitals, the electron has a net angular momentum due to the nature of its orbit around the nucleus; and (2) a contribution due to the spin of the electron. The orbital contribution can be simply thought of as arising from the fact that while the electron is orbiting around the nucleus, it travels in a loop. This is similar to a current-carrying loop of wire, which has a magnetic moment $m = IA$, where I is the current and A is the area of the loop. The spin angular momentum is an intrinsic property of the electron.

Ultimately, it is the interplay between the spin and the orbital magnetic moments in materials that gives rise to the various types of magnetic behaviour that we observe and take advantage of in our everyday lives. We use magnets for a variety of applications including motors and generators (without which we would probably not have electrical power), levitation bearings, and magnetic reso-

nance imagers to name a few. The magnetic properties of bulk magnets are well known and understood on the 10 micron scale and above, as it is relatively easy to both fabricate and characterize magnets made from a variety of materials. As the scale of magnets goes down, however, to sub-micron dimensions, the rules governing their properties become quite complex. This in turn is due to the interplay between the dipolar interaction [2] which is a long-range force tending to align magnetic dipoles antiparallel to each other, and the exchange interaction which acts at short range, and tends to align dipoles parallel (see figure 2). The characteristic distance over which this interaction is important, the exchange length, is of the order 5 nm, so when magnetic materials are patterned with dimensions in the range 1–100 nm, their magnetic properties are dominated by the shape and symmetry of the magnet. This so-called 'configurational anisotropy' has been studied at length in recent years, and is starting to pave the way for a whole new class of memory storage and computational devices [3–8]. An example of a nanomagnetic structure is shown in figure 3, which is a magnetic force microscope (MFM) image of an indented square nanomagnet with a vortex core at the centre. This vortex arises because the magnetization takes on the symmetry of the nanomagnet (configurational anisotropy), and is therefore directed circularly. The principle of operation of MFM is that we scan a sharp magnetic tip over the surface we are interested in, at a height of a few tens of nanometres. These tips are generally magnetized along the tip axis, and if the sample is magnetized along the same axis, there will be a force between them, like the force between two bar magnets. Depending on whether the tip and sample magnetizations are aligned parallel or antiparallel, the resultant force will

Author's address: Nanoscience, University of Cambridge, 11 J. J. Thompson Avenue, Cambridge, CB3 0FF. e-mail: cd229@eng.cam.ac.uk
www: <http://www.eng.cam.ac.uk/~cd229/>

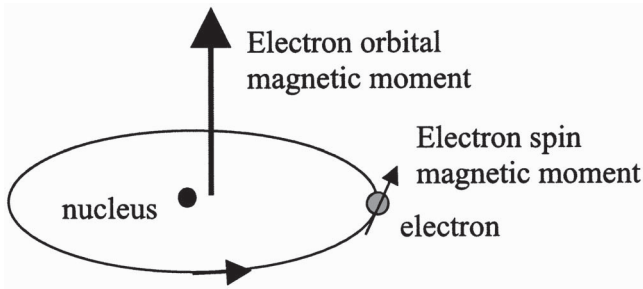


Figure 1. Schematic of orbital and spin magnetic moments.

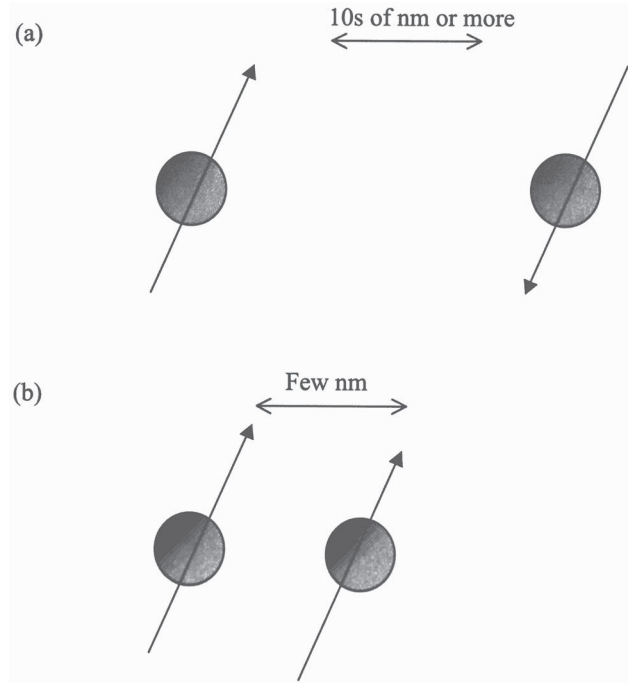


Figure 2. (a) At long range, the dipolar interaction tends to align magnetic moments antiparallel, and (b) at short range, the exchange interaction lines them parallel.

be either attractive or repulsive, respectively. Simply by measuring this force as the tip is raster scanned across the surface, we can spatially map out the magnetization of the sample. At the centre, the magnetization is simultaneously trying to point in all directions in the plane of the surface. The only way this can be achieved is for the magnetization at the very centre to point out of the plane (hence the name vortex). This is analogous to the way water exits through a plughole! This type of structure has some technological relevance, as we shall see later.

At the same time as these novel magnetic devices with nanometre length scales are emerging, conventional magnetic data bits are continuing to shrink. A data bit in a hard disk currently looks rather like a 2-D bar magnet, with

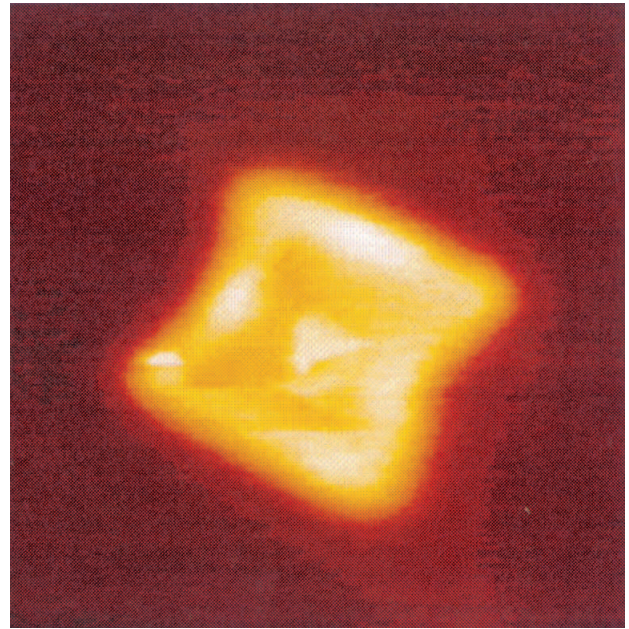


Figure 3. MFM image ($1000 \text{ nm} \times 1000 \text{ nm}$) of nanomagnet with a vortex at the centre (bright spot).

dimensions around $100 \times 1000 \text{ nm}$. As these bits continue to be made smaller, there comes a point at which they can no longer store information—the superparamagnetic limit [9]. The way in which these bits store information is in their magnetization: we assign one direction of magnetization as a logical ‘0’, and the opposite direction as a ‘1’. In order to switch the magnet from a 0 to a 1 or vice versa (i.e. to write information), we must apply a field greater than the coercive field. This implies we need to input energy. For a data storage structure to be technologically useful, this switching energy must be much greater than the thermal energy ($k_B T$) of the environment (thermal energy tends to randomize spins). As magnets shrink, this energy decreases, and the size at which magnets become thermally unstable is of the order a few nanometres. The MFM image of figure 3 shows a structure with a vortex at the centre, which essentially makes this structure useless for data storage. A lot of work has been done recently which shows that by tailoring the shape and size of nanomagnets, the magnetic properties can be tailored over a wide range of different regimes, and there are configurations for which there is no vortex core [10]. An aim therefore of nanomagnetic research is to overcome the superparamagnetic limit by understanding what happens when we pattern magnetic materials down to the 10 nm level. As a direct consequence of this, it is becoming crucial to be able not only to fabricate but also to locally characterize (image) magnetic structures with a spatial resolution of well below 10 nm. Unfortunately, this is outside the realm of MFM, which can only attain a resolution of around 10 nm in the best

case [11, 12]. An obvious technique to consider then is scanning tunnelling microscopy (STM) [13], as this is a technique which can be used routinely to obtain atomic-scale images of conducting surfaces. STM is a member of the family of scanning probe microscopes that have revolutionized the area of nanotechnology. To see why, we should consider that with the current advances in nanoscale science and technology, it is becoming increasingly important to be able to characterize materials at the nanometre scale and below. This has largely been made possible through advances in scanning probe microscopy techniques. Using these techniques, one can obtain information about the shape and size of nano- to microstructures, as well as material and electronic properties such as friction coefficient, stiffness, optical absorption, density of electronic states, distribution of surface potential, and magnetization [14]. However, despite the tremendous advances that have been made, it is generally very difficult to conclusively distinguish between materials at the atomic scale. This is mostly due to the complex nature of image formation in STM. If we had a magnetic-sensitive STM, then in principle we would be able to map out the magnetization of surfaces with unprecedented spatial resolution. This has been demonstrated rather spectacularly in recent years, in the form of spin-polarized STM (SPSTM) [15–22]. The principle of SPSTM is illustrated in figure 4. A magnetic STM tip emits spin-polarized electrons, and then when those electrons encounter a surface, the net current will be reduced if the sample is magnetized in the opposite direction to the tip, and increased if it is in the same direction. This technique has already demonstrated atomic spatial resolution.

Continuing along the same vein then, if we could combine the atomic spatial resolution of STM with spin sensitivity, we could hope to map out the spin states of structures at the atomic level.

Recent work has shown that it is possible to extend the capabilities of STM to be able to detect single magnetic entities on surfaces, and determine a method by which one can distinguish between different magnetic elements at the atomic scale, by measuring their electronic spin [23]. The importance of this is down to the far-reaching implications of being able to perform measurements on single magnetic atoms/molecules. This opens up opportunities for investigating the interactions between individual spins, which may one day be of use to (i) the magnetic data storage industry as data densities continue to increase, and (ii) the future of solid-state quantum computation.

One problem is immediately obvious—the *lower* limit to detection of electronic spins by conventional methods is of the order 10^{10} spins, so how can we hope to detect single spins? In recent years, a variety of techniques have been used to detect the presence of small numbers of spins, including optically detected magnetic resonance (ODMR)

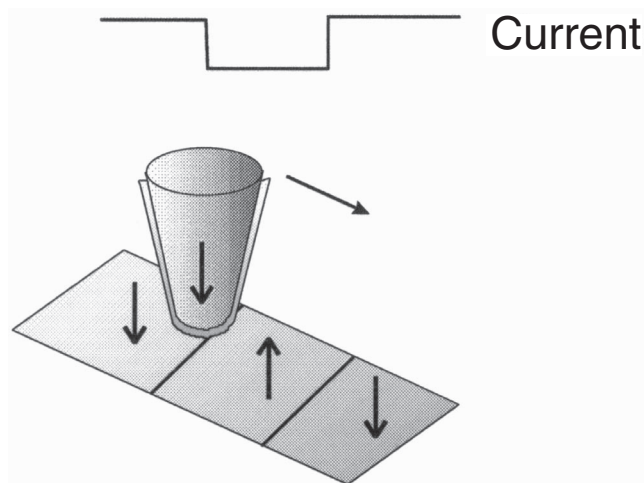


Figure 4. Principle of SPSTM. Top trace shows typical variation in tunnel current as tip passes over regions of alternate magnetization. Arrows in tip and sample represent direction of magnetization. The coating on the tip represents a magnetic thin film.

[24], magnetic resonance force microscopy (MRFM) [25, 26] and Superconducting Quantum interference devices (SQUIDs) [27]. The development of these techniques to this level of sensitivity has been driven by the desire to build a solid-state quantum computer.

While these new techniques are extremely promising, they suffer from the drawback of having poor spatial resolution. It is for this reason that we wished to combine the sub-nanometre spatial resolution of STM with single-spin sensitivity. Conventionally, spins are detected by electron-spin resonance (ESR), whereby a static magnetic field is applied to a sample, and this causes the spins to align with the applied field. Some of them will align parallel to the field, and the others will align anti-parallel to it. There will be a difference in energy between these two states, called the Zeeman energy (i.e. their frequency is the Larmor frequency), they will be absorbed by the sample. Simply by monitoring this absorption at a given frequency as a function of applied magnetic field strength, we can extract quite a lot of information about the nature of the spins in the sample. While this is a very useful technique, which is used routinely in materials science and chemistry research, it has no spatial resolution, and can only detect at least 10^{10} spins.

To detect single spins by STM, the measurement technique entails applying a small DC magnetic field to a sample that is in an STM system. This field will cause all free, unpaired electrons to precess at the Larmor frequency (ν_L). Using an STM tip to tunnel into magnetic regions of the sample, this spin precession gives rise to a radio frequency (RF) modulation of the tunnel current, whose frequency ν_L ,

depends on the sample g -factor and the applied magnetic field ‘ B ’, in the manner $\nu_L = g\mu_B B/h$, where μ_B is the Bohr magneton, and h is Planck’s constant. By detecting this RF signal with a spectrum analyser, it is possible to locate single electronic spins on surfaces, detect spin–spin coupling and spin–surface coupling, and obtain local spectroscopic information. As well as its potential use for quantum computation, this technique could ultimately also lead to a way of distinguishing between materials at the atomic level.

The technique of STM-based single-spin detection is not actually that new. Yishay Manassen and his group originally developed and have continued to work with this technique since 1989 [28–31]. An alternative technique developed by Dalidchik, and based on exchange splitting of field emission spectra has also shown some promise for the detection of single spins [32, 33]. Previous experiments have already demonstrated to some extent the principle described above, by detecting (i) spin centres on Si and (ii) iron islands on Si. In the next section, we consider some experiments demonstrating the efficacy of this technique.

2. Experimental

In our work, we chose to study molecular systems which are well known from conventional ESR experiments. This included the organic molecules, BDPA (α,γ -bisdiphenylene β -phenylallyl) and TEMPO, both of which contain free radicals [34, 35]. These free radicals give rise to a large spin signal, which therefore make them an ideal candidate for test experiments. It is also known that both molecules have no orbital angular momentum ($l = 0$), and TEMPO has a nuclear spin (denoted by I , which in this case = $\frac{1}{2}$), and hence exhibits hyperfine splitting.

In order that the substrate itself does not interfere with the experiments, it must not contain any free spins. For that reason, we chose highly oriented pyrolytic graphite (HOPG). This is also suitable due to the fact that (1) atomic resolution is more or less routine under ambient conditions and (2) spin–orbit coupling in this material is

negligible. We will now consider the experiments on the two different molecules separately.

2.1 Spin detection in BDPA molecules: $s = \frac{1}{2}$, $l = 0$, $I = 0$

The samples are prepared by dissolving crystals of BDPA in Isopropanol, and applying a drop of the resulting solution to a substrate. When this dries, it leaves the molecules dispersed on the surface. The coverage can be controlled by changing the volume and/or concentration of solution applied to a given area of substrate. We typically used a concentration that results in a mean coverage of a few hundred molecules per square micron. This deposition process generally leaves the molecules in clusters ranging in size from 50–500 nm, as well as a smaller proportion of monodisperse molecules.

To make the spins precess, an externally applied magnetic field is required. We tried a number of different configurations from permanent magnets to electromagnets, and found that the most convenient method was simply to mount the sample on a small Sm/Co permanent magnet. The sample is mounted on the magnet in such a way that the field is parallel to the tip axis. The field strength at the sample surface was varied from 190 G to 300 G (as measured by a Hall probe) by using a range of magnet sizes. The corresponding theoretical Larmor frequency is in the range 538–840 MHz, assuming a g -factor of 2.0. It is essential to have an accurate measure of the field strength, in order to be able to select the appropriate frequency range of the spectrum analyser. The accuracy of the Hall probe we used was 0.1 G, which is equivalent to 0.28 MHz uncertainty in the peak position. It must be taken into consideration that there are many external RF sources in the frequency range between 100 MHz and 1 GHz—mainly mobile phones. Therefore, great care must be taken to adequately shield the STM system from these sources of ‘noise’. In our case, this was done by using microwave cable to carry the tunnel current to the RF amplifier, and the entire STM was encased in a steel and copper case.

The experimental set-up is as shown in figure 6. In order to measure the spin signal, it is necessary to split the tunnel current into two pathways: one which goes to a 50 Ω impedance-matched RF amplifier, and the other which goes to a conventional high-gain current–voltage converter for STM distance regulation. The RF signal is then detected with a spectrum analyser. The spectrum analyser used in these experiments has a noise floor of -131 dbm [36]. We found that with this set-up the lowest tunnel current that we could use without significant image degradation was approximately 200 pA. For all experiments, either electrochemically etched Pt–Ir or mechanically formed Au tips were used. The HOPG was freshly cleaved immediately before any deposition.

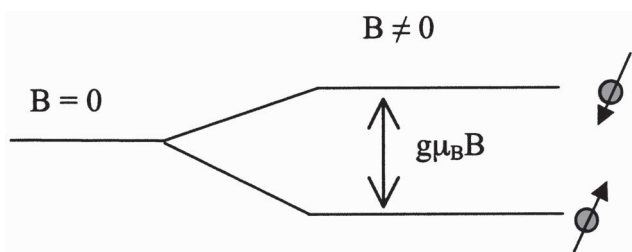


Figure 5. A magnetic field removes the degeneracy of free spins, i.e. they split in energy, depending on whether they have spin-up or spin-down (i.e. they are parallel or anti-parallel to the field direction).

BDPA molecules were deposited on the HOPG, by dissolving them in Isopropanol, placing a drop on the sample, and allowing it to dry for 30 min. The sample was then imaged to locate molecules, and the tip was held at various locations while spectra were obtained. Figure 7 shows an STM image ($250 \text{ \AA} \times 150 \text{ \AA}$) of a sample prepared in this way showing single molecules. From our STM images, these molecules have apparent dimensions of the order $40 \text{ \AA} \times 60 \text{ \AA}$, and are $2\text{--}3 \text{ \AA}$ high. For a magnetic field of 190 G, RF modulations appeared in the tunnel current in the frequency range 533–539 MHz, as shown in figure 8. Typically, a peak would appear at a given frequency and last for about 100 ms–1 s, and then disappear. The spectra as obtained by the spectrum analyser were measured every 40 ms. Occasionally another peak then appears at a slightly different frequency, but the peaks are always within a few megahertz of each other. Spectra taken when the tip is halted above HOPG show no evidence of any peaks, as is shown in figure 8.

In a number of cases, the spectra were much less sharp than those shown. This is likely to be due to the arrangement of molecules on the surface in clusters. The sharper the spectra, the fewer molecules are in the cluster.

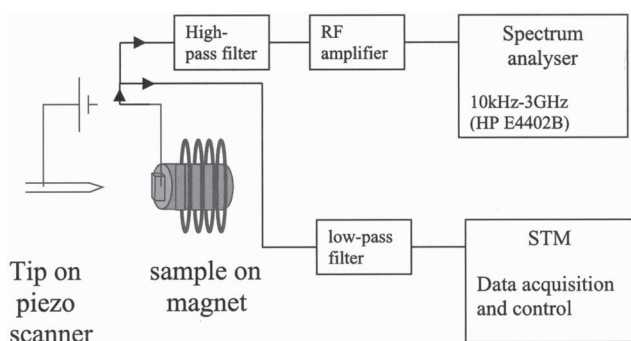


Figure 6. Schematic of experimental apparatus used for spin detection.

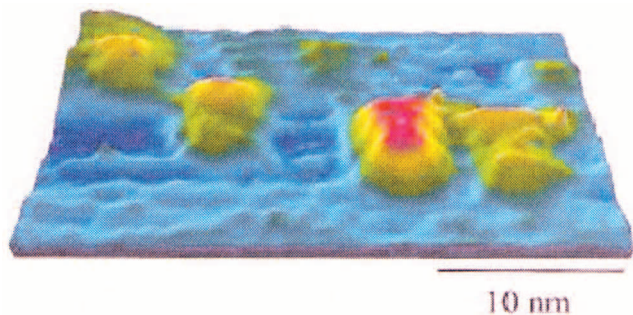


Figure 7. STM image of $25 \text{ nm} \times 15 \text{ nm}$ area of HOPG surface, showing four adsorbed BDPA molecules (raised features in green and red).

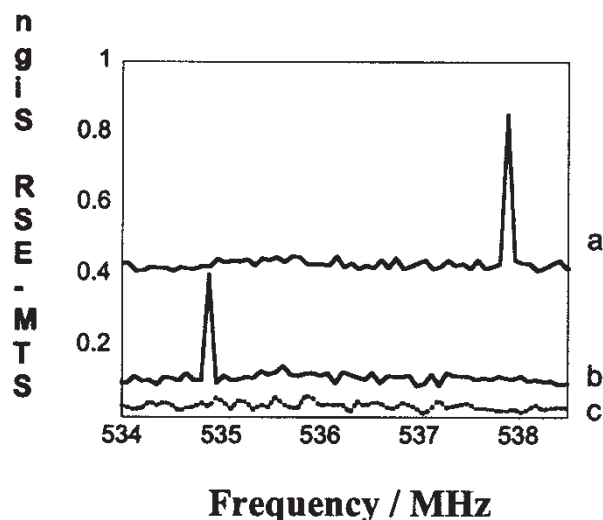


Figure 8. STM spin spectra of (a), (b) two different areas (a few nanometres apart) of the molecule-covered sample, and (c) bare HOPG. The graphs are shifted vertically for clarity.

The fact that there is (a) a modulation of the tunnel current at the Larmor frequency when tunnelling into a molecule and (b) no evidence of any modulation when tunnelling into HOPG indicates spin sensitivity. In order to rule out spurious signals and further corroborate the effect, we have conducted a study of the magnetic field dependence of the RF peak position. The field was changed to 210 G and then 285 G by changing the permanent magnet on which the sample was placed, and the corresponding central frequencies of the observed peaks were measured. It must be stressed that this procedure makes it impossible to investigate the same molecular cluster every time. Figure 9 shows two different spectra at 210 and 285 G showing that the frequency does indeed increase with applied field strength. The observed variation in frequency with applied field is much greater than the apparent random variation between clusters, which is a few megahertz. These spectra are rather broader than those of Figure 8, as these measurements were performed on clusters rather than on single molecules. We also notice the trend that the linewidth increases with increasing frequency, in a manner which is consistent with that found in [29] for defects in SiO_2 . The origin of this frequency-dependent linewidth is not yet fully understood, although we believe that it is related to the fact that we are sampling the precession of the spins via uncorrelated tunnelling events, which should give a Poissonian lineshape.

The linearity of the observed relationship between peak frequency and applied field is illustrated in figure 10. Using the earlier expression for Larmor frequency and knowing the accuracy of the magnetic field measurement, we obtain a value for g of 2 ± 0.1 .

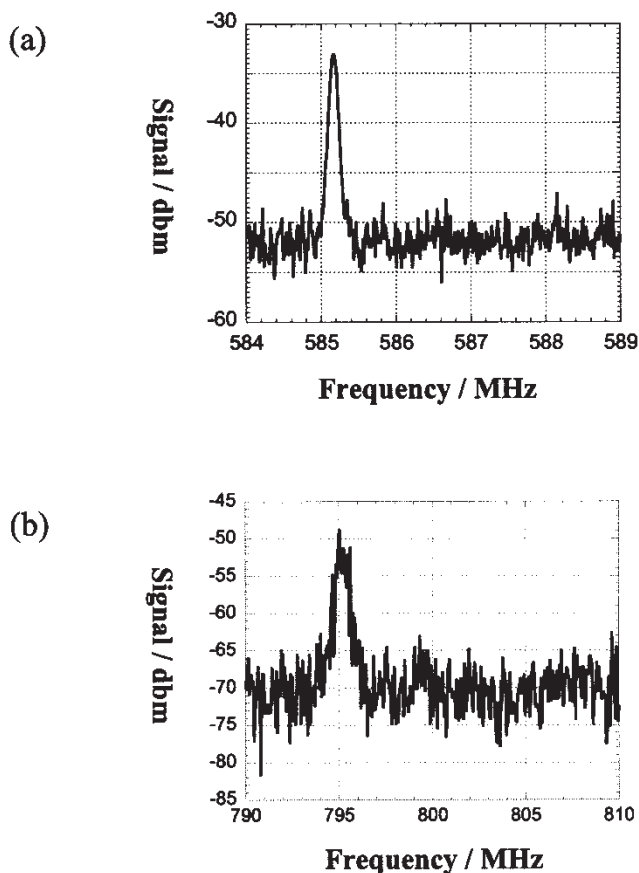


Figure 9. STM spin spectra of BDPA clusters for applied fields of (a) 210 G and (b) 285 G.

2.2 Spin detection in TEMPO molecules: $s = \frac{1}{2}$, $l = 0$, $I = \frac{1}{2}$

Now we see that we can detect single spins, what else can this technique do? Another important and useful capability to have, particularly for quantum computing applications is the ability to detect *nuclear* spins. If this technique is sensitive to electronic spins, then we should be able to detect nuclear spins via the hyperfine interaction. Briefly, the hyperfine interaction is whereby the nuclear spin produces a magnetic field which Zeeman splits the electronic levels. So, if we have an electronic spin-half system with hyperfine splitting, in an external magnet field each electronic level will be split into a number of sub-levels, the number of these depending on the spin of the nucleus. If we then do an ESR measurement, we will now see several peaks corresponding to transitions between the various hyperfine levels.

The molecule we chose to study was TEMPO—an inorganic free radical found in nerve cells, and one whose ESR characteristics have already been studied in the solid state [37]. For STM studies on these molecules, samples were prepared in the manner already described. An STM

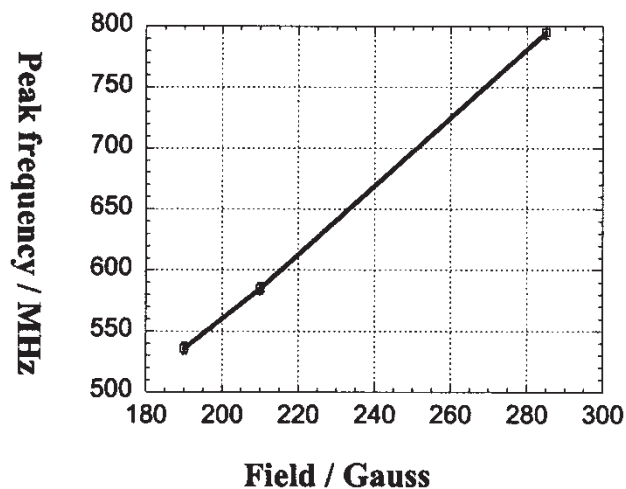


Figure 10. Plot of central frequency of STM spin spectra peaks on clusters as a function of the applied magnetic field. From this, we obtain a value of $g = 2 \pm 0.1$.

image of a large cluster of molecules is shown in figure 11. A typical STM spin-spectrum is shown in figure 12. There are three main features to note: (i) there are three peaks; (ii) the frequency of the central peak corresponds to the Larmor frequency for the value of B which was used; and (iii) the spacing between the peaks is not equal—spacings of 29 MHz and 25.7 MHz were measured. This is in very close agreement with conventional ESR results obtained elsewhere for this molecule [37]. This is clear evidence that this technique is indeed capable of detecting electronic and even nuclear spins.

Having discussed the experimental evidence demonstrating the efficacy of this technique, we must now consider the theoretical basis behind it.

3. Theory

This is a complicated theoretical issue, and many differing models have been proposed to date to explain the origin of the spin-sensitive signal. As a starting point, we need to consider how *strong* the effect is. In other words, how large is the modulation of the tunnel current at the Larmor frequency? To answer that question, we need to consider the exact nature of the measurement setup. The RF component of the tunnel current is amplified with an amplifier of gain 24 dB, and the magnitude of the spin signal for single molecules is of the order 3 mV. This means the voltage at the input to the amplifier must be around 200 nV. However, this is a voltage amplifier rather than a current amplifier, so we need to know how much current our 200 nV corresponds to. Given that the cables carrying the RF signal to and from the amplifier have an impedance of 50 Ω , and that the amplifier itself is also 50 Ω matched, it

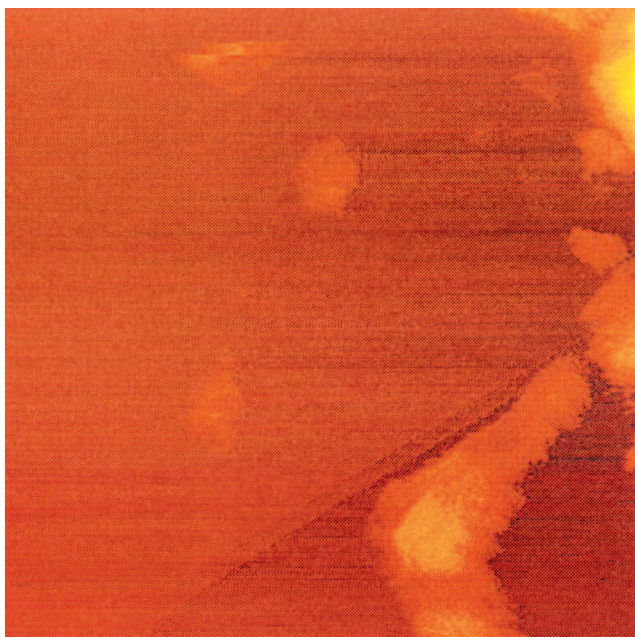
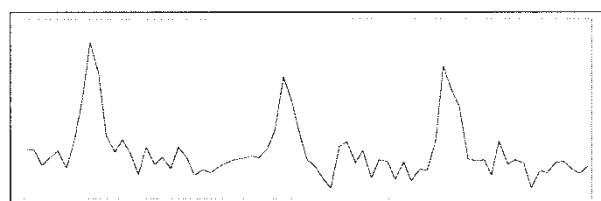


Figure 11. STM image of $25 \text{ nm} \times 25 \text{ nm}$ area of HOPG surface, showing adsorbed clusters of TEMPO molecules.



485 525 575
Frequency / MHz

Figure 12. STM spin spectra of TEMPO clusters, from which we can clearly see three peaks—evidence of hyperfine splitting.

has an extremely high resistance associated with it. In effect therefore, it acts as an ideal current source, and transmission-line effects can essentially be neglected. The resistance and capacitance of a typical tunnel junction are $2 \times 10^8 \Omega$ and 10^{-18} pF , respectively, so to a first approximation, we can say that 200 nV is due to a current of around 10^{-15} A . Given that the dc tunnel current we typically use is around 1 nA, this is a very small effect—1 in 10^6 ! Also, if we take the somewhat simplistic but nonetheless instructive view that a tunnel junction is a resistance in parallel with a capacitance, we obtain an electronic time constant of about 1 ns, meaning that it would be difficult to measure signals much higher than 1 GHz or so. If we wanted to do so, we would have to change either the resistance or capacitance of

the tunnel junction. This can be done rather easily, as the resistance scales inverse exponentially with the tip–sample distance, whereas the capacitance scales directly with the tip–sample distance. Therefore, moving the tip closer to the surface will allow us to increase the frequency response of the tunnel current. In reality, tunnelling happens at the single-electron level, and the time taken for an electron to tunnel across a typical junction is of the order a femtosecond.

Armed with this knowledge about the magnitude of the spin signal, we need to now consider what its possible origin may be. As a starting point, let us consider a simple tunnelling junction in the presence of an applied voltage bias and a magnetic field, as illustrated in figure 13. The effect of the applied bias is to introduce a slope to the barrier and shift the Fermi levels on both sides. We include the slope by means of the WKB method [1]. The mean energy of the tunnelling electrons is the Fermi energy. The effect of the magnetic field will be to cause a certain number of the electrons to have a slightly higher energy (spin anti-parallel to the applied field—spin *down*) and the rest will have a slightly lower energy than this (spin parallel to the applied field—spin *up*). The shifts in energy due to the magnetic field are just $\pm g\mu_B B$, and the occupation probability of electrons in the spin down and the spin up states is given by the Fermi–Dirac factor which is $1/(1 + e^{g\mu_B B/kT})$, where k is the Boltzmann constant and T is the temperature. What we are interested in initially is to see what proportion of the tunnel current is spin polarized. We do this by

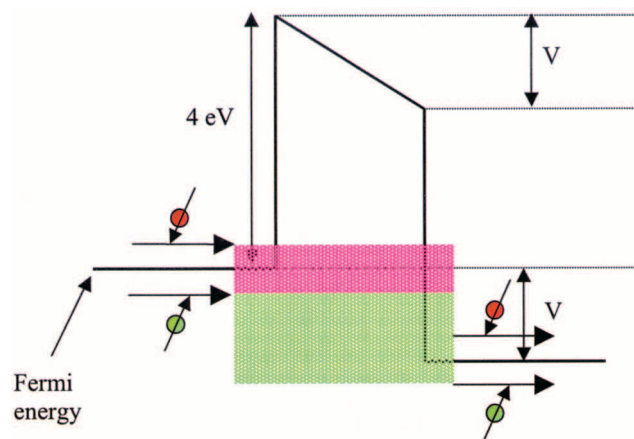


Figure 13. Tunnelling barrier geometry used in calculations. The tip is on the left, and the sample is on the right. An applied voltage bias between the two causes the barrier to slope, and the Fermi levels to shift. An applied magnetic field B causes the spins to fall into either spin up (green) or spin down (red). The tunnel current is calculated by integrating the transmission probability for spin up and spin down electrons separately over the states indicated by the shaded regions—green and red, respectively.

considering spin-up and spin-down electrons separately. As figure 13 shows, each type of spin can tunnel into a range of states indicated by the shaded regions. In each case, these states are between the electron's initial energy (they can't tunnel into higher energy states—conservation of energy), and the Fermi level on the right-hand side (states below the Fermi energy are filled, so can't be tunnelled into either). In the absence of an applied magnetic field, and for a non-magnetic tip and sample, the tunnel current should have no net spin—there will be equal numbers of electrons with spin up and spin down. However, when we apply a magnetic field, by virtue of the Fermi–Dirac factor we shift this balance, and we will end up with some more electrons in the spin-up state (as it is the lower energy state). The larger the Zeeman splitting energy is relative to kT , the larger the imbalance will be, and hence the tunnel current will have a degree of spin polarisation. For our simple simulation, we assume that the tunnelling barrier has a height of 4 eV, a width of 0.7 nm (typical distance between a tip and a sample in STM), and an applied magnetic field of 200 gauss (20 mT), at room temperature (300 K). The tunnel current as a function of voltage is given by the expression:

$$I = \frac{2e}{h} \int_{eV}^0 T(E, V) [F_t(E, V) - F_s(E, V)] dE \quad (1)$$

where F_t and F_s are the Fermi functions of the tip and sample, respectively, and $T(E, V)$ is the quantum-mechanical probability of an electron tunnelling through the barrier—which we calculate numerically using the WKB method. In figure 14 we show the calculated spin up and spin down currents, and in figure 15, we show the degree of spin polarization (spin down current–spin up current)/(spin down current + spin up current). What we can immediately see is that for our situation, the degree of polarization is around 6.5×10^{-5} . This corresponds to a spin-polarized current of 65 fA, which is somewhat larger than that which we measure. However, we must remember the fact that our estimate of the magnitude of the effect was extremely crude, and the experimental apparatus will not be perfect. We must also remember that what we are calculating here is the dc proportion of the tunnel current which is spin polarized, rather than the ac component (which is what the experiments measure). Due to the way in which we split the tunnel current, we are limited to detecting around half of the RF component which is present. As well as that, if there is an angle θ between the spin of the tunnel current and the magnetic entity we are probing, that will modify the current by a factor $1/(1 + \cos\theta)$. If we assume that the molecule we are tunnelling into has a spin whose direction is random, then taking into account both of these factors, we would expect

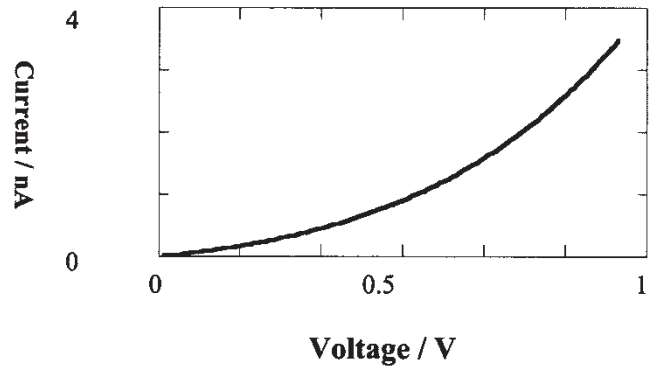


Figure 14. Calculated I – V characteristics for a 4 eV tall barrier which is 0.7 nm wide, in the presence of a magnetic field of strength 200 G, at room temperature. There is no discernible difference between the spin up and spin down currents.

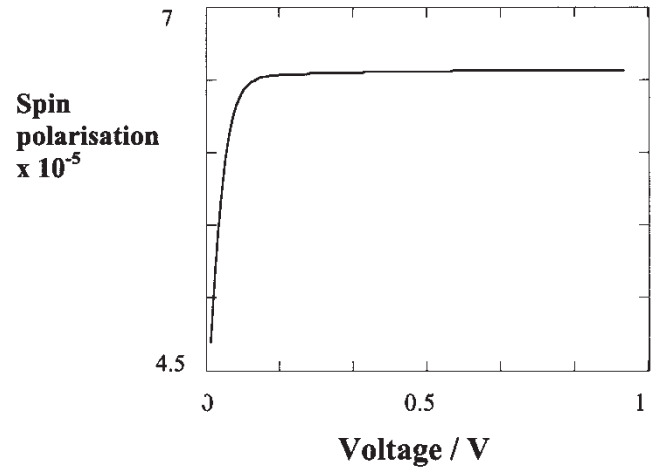


Figure 15. Degree of spin polarization of current as a function of applied voltage, for the same barrier conditions as in figure 14.

a time-averaged dc spin signal of around 20 fA. If the spin of the molecule is precessing coherently, we would expect the tunnel current to be modulated at that precession frequency—the Larmor frequency. If the tip is sitting directly above the spin, we would expect there to be no modulation, as the component of the spin along the direction of the tunnel current's spin is unchanging. As we move away from the spin, we would expect to start seeing a modulation in the tunnel current, which will decay exponentially as we move further away from the spin. Qualitatively, this will give a sinusoidal function superimposed with an exponential decay, as schematically illustrated in figure 16. The decay with distance has been observed, although not correlated exactly with the position of the spin [28]. There will also be losses in the cables due to their resistance and the fact that there will not be perfect

impedance matching everywhere (we can only neglect that to a first approximation). We can easily imagine that these losses would be large enough to bring convergence between our measurements and this simple model.

Of course, the exact nature of the interaction between the spin of the tunnel current and the spin of the molecule is still unknown. It is not at all clear how the spin of the molecule could be precessing coherently for a long enough time for a measurement to be made. In our case, the frequency range over which we observe this effect is scanned in about 0.1 ms, which corresponds to 50 000 precessions. It has been reported in the literature that there may be an element of spin–orbit coupling, where the spin of the molecule couples to the orbital motion of electrons in the underlying substrate [38]. This will modulate the density of states of the molecule at the Larmor frequency, and hence will be detectable by STM. Our experiments tend to rule that out, as there is negligible spin–orbit coupling in the substrates we used. Another possibility is that there is spin–orbit coupling introduced by the surface itself. An alternative mechanism that has been proposed is that the spin of the tunnelling electron interacts with the molecular spin via the exchange interaction [39–41]. This amounts to the spin being detectable due to the manner in which it alters the tunnelling current noise at the Larmor frequency.

Both of these models can offer explanations as to the origins of the spin signal that we observe experimen-

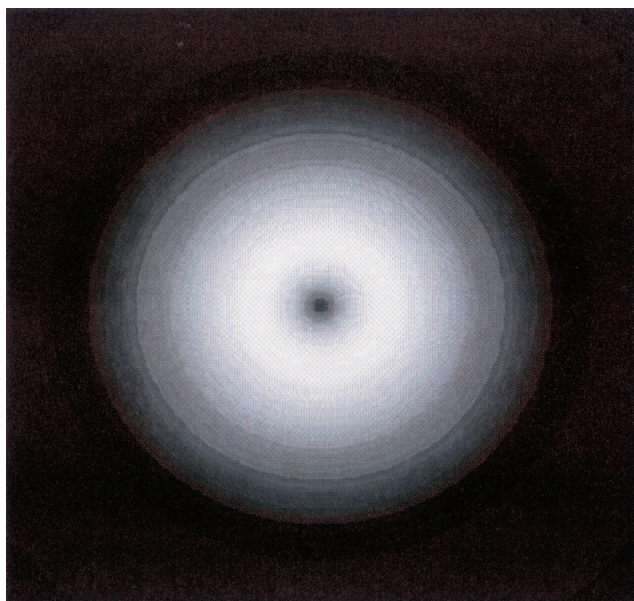


Figure 16. Qualitatively expected dependence of spin signal on position, for a precessing spin located at the centre. Scale is in arbitrary units.

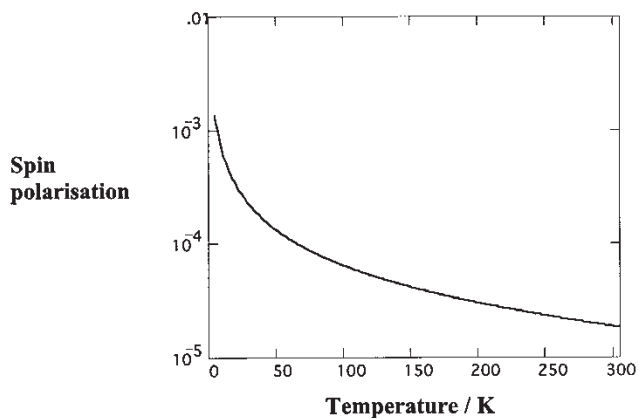


Figure 17. Calculated dependence of spin polarization on temperature.

tally, but both are still somewhat controversial. Until a robust theoretical framework has been established, our simple model will continue to be useful. Three things which are clear from our model are (i) as the tunnel current is increased, the proportion of it which is spin-polarized will remain the same, so that magnitude of the spin signal should effectively scale linearly with the tunnel current; and the degree of spin polarization should increase (ii) as the temperature is decreased (see figure 17), and (iii) as the magnetic field strength is increased. What this is all pointing towards is the need to perform spin-detection experiments at cryogenic temperatures—something which we are currently working towards.

4. Conclusions

In conclusion, we have demonstrated that STM may be used to detect single electronic spins and even nuclear spins (via the hyperfine interaction). This has been demonstrated on two different types of molecule, under ambient conditions. We have also briefly considered the physical origin of this effect, and find that it may be due to the fact that a very small proportion of the tunnel current is spin-polarized in the presence of a magnetic field. While a number of publications in the literature have proposed various schemes whereby this effect can be explained, we feel that there is not enough experimental evidence to be able to strongly support any of them as yet.

Acknowledgements

This work has been supported by the EPSRC and the EU. The latter is via the IST project “QIPDDF-ROSES”.

References

- [1] See for instance, Townsend, J. S., 1992, *A Modern Approach to Quantum Mechanics*, (Singapore: McGraw-Hill).
- [2] Jackson, J. D., 1998, *Classical Electrodynamics*, 3rd edition (USA: Wiley).
- [3] Koltsov, D. K., Cowburn, R. P., and Welland, M. E. 2000, *J. Appl. Phys.*, **88**, 5315.
- [4] Cowburn, R. P., Koltsov, D. K., Adeyeye, A. O., and Welland, M. E., 2000, *J. Appl. Phys.*, **87** (9), 7082.
- [5] Cowburn, R. P., and Welland, M. E., 2000, *Science*, **287**, 1466.
- [6] Cowburn, R. P., 2000, *J. Phys. D*, **33**, R1.
- [7] Cowburn, R. P., Adeyeye, A. O., and Welland, M. E., 1999, *Europhys. Lett.*, **48**, 221.
- [8] Allwood, D. A., Xiong, G., Cooke, D., Faulkner, C. C., Atkinson, D., Vernier, N., and Cowburn, R. P., 2003, *Science*, **296**, 2003.
- [9] See for instance, Koltsov, 2002, PhD thesis, University of Cambridge.
- [10] Koltsov, D. K., and Welland, M. E., 2003, *J. Appl. Phys.*, **94**, 3457.
- [11] Wickramasinghe, H. K., 1990, *J. Vac. Sci. Technol.*, **8**, 363.
- [12] Shinjo, T., Okuno, T., Hassdord, R., Shiegt, K., and Ono, T., 2000, *Science*, **290**, 930.
- [13] Binnig, G., and Rohrer, H., 1982, *Helv. Phys. Acta*, **55**, 726.
- [14] Pohl, D. W., 1992, *Scanning Tunneling Microscopy II*, edited by R. Wiesendanger and H. J. Güntherodt (Berlin: Springer-Verlag), 233.
- [15] Wachowiak, A., Wiebe, J., Bode, M., Pietzsch, O., Morgenstern, M., and Wiesendanger, R. 2002, *Science*, **298**, 577.
- [16] Kubetzka, A., Pietzsch, O., Bode, M., and Wiesendanger, R., 2003, *Phys. Rev. B*, **67**, 020401.
- [17] Bode, M., Heinze, S., Kubetzka, A., Pietzsch, O., Nie, X., Bihlmayer, G., Blügel, S., and Wiesendanger, R., 2002, *Phys. Rev. Lett.*, **89**, 237205.
- [18] Kubetzka, A., Bode, M., Pietzsch, O., and Wiesendanger, R., 2002, *Phys. Rev. Lett.*, **88**, 057201.
- [19] Pietzsch, O., Kubetzka, A., Bode, M., and Wiesendanger, R., 2001, *Science*, **292**, 2053.
- [20] Kleiber, M., Bode, M., Ravlic, R., and Wiesendanger, R., 2000, *Phys. Rev. Lett.*, **85**, 4606.
- [21] Heinze, S., Bode, M., Kubetzka, A., Pietzsch, O., Nie, X., Blügel, S., and Wiesendanger, R., 2000, *Science*, **288**, 1805.
- [22] Pietzsch, O., Kubetzka, A., Bode, M., and Wiesendanger, R., 2000, *Phys. Rev. Lett.*, **84**, 5212.
- [23] Durkan, C., and Welland, M. E., 2002, *Appl. Phys. Lett.*, **80**, 458.
- [24] Kennedy, T. A., Freitas, Jr., J. A., and Bishop, S. G., 1990, *J. Appl. Phys.*, **68**, 6170.
- [25] Stipe, B. C., Mamin, H. J., Yannoni, C. S., Stowe, T. D., Kenny, T. W., and Rugar, D., 2001, *Phys. Rev. Lett.*, **87**, 227602.
- [26] Rugar, D., Yannoni, C. S., and Sidles, J. A., 1992, *Nature*, **360**, 563.
- [27] Granta, C., Corato, V., Longobardi, L., Russo, M., Ruggiero, B., and Silvestrini, P., 2002, *Appl. Phys. Lett.*, **80**, 2952.
- [28] Manassen, Y., Hamers, R. J., Demuth, J.E., and Castellano, A. J., 1989, *Phys. Rev. Lett.*, **62**, 2531.
- [29] Manassen, Y., Ter-Ovanesyan, E., Schachal, D., and Richter, S., 1993, *Phys. Rev. B*, **48**, 4887.
- [30] Manassen, Y., 1997, *J. Magn. Reson.*, **126**, 133.
- [31] Manassen, Y., Mukhopadhyay, I., and Ramesh Rao, N., 2000, *Phys. Rev. B*, **61**, 16223.
- [32] Dalidchik, F. I., and Kovalevskii, S. A., 1998, *JETP Lett.*, **67**, 965.
- [33] Buchachenko, A. L., Dalidchik, F. I., and Shub, B. R., 2001, *Chem. Phys. Lett.*, **340**, 103.
- [34] Supplied by Sigma-Aldrich.
- [35] Dalal, N. S., Kennedy, D. E., and McDowell, C. A., 1974, *J. Chem. Phys.*, **61**, 1689.
- [36] HP E4402b, Agilent technologies, UK.
- [37] Hubbel, W. L., and McConnell, H. M., 1968, *Proc. Natl. Acad. Sci. USA*, **61**, 12.
- [38] Zhu, J. X., and Balatsky, A. V., 2002, *Phys. Rev. Lett.*, **89**, 286802.
- [39] Balatsky, A. V., Manassen, Y., and Salem, R., 2002, *Phys. Rev. B*, **66**, 195416.
- [40] Nussinov, Z., Crommie, M. F., and Balatsky, A. V., 2003, *Cond. Matter*, /0301032.
- [41] Bulaevskii, L. N., Hruska, M., and Ortiz, G., 2002, *Cond. Matter*, /0212049.